JOURNAL OF MATERIALS SCIENCE 20 (1985) 4335–4344

# The structure of stircast Al–6Cu*

J. M. M. MOLENAAR, F. W. H. C. SALEMANS, L. KATGERMAN
*Laboratory of Metallurgy, Delft University of Technology, Rotterdamseweg 137, 2628 AL Delft, The Netherlands*

A series of batch-type stirring experiments have been performed to investigate the morphological changes in the growth of the primary solid phase in Al–6Cu (Al–6 wt% Cu), as a function of the cooling rate and the rotational speed of the stirrer. The experiments show, that the cell-spacings of primary particles in stircast microstructures increase as a result of stirring, when compared to secondary dendrite arm spacings in the unstirred alloy. This result can be explained regarding heat transport during solidification. It is suggested that the solid–liquid interface of floating crystals in bulk metal liquids is cellular.

## 1. Introduction

Stircasting (also termed rheocasting) is a casting process, in which metal slurries are cast at temperatures in the liquidus–solidus region, under mechanical stirring [1]. From extensive investigations of the behaviour and structure of semi-solid metal slurries [2–5], the most important observations were: (1) when metal alloys are vigorously agitated during solidification, the solid which forms has a special non-dendritic structure, (2) semi-solid metal slurries behave as thixotropic fluids.

During stircasting, the solidification takes place in two stages. In the first stage, the solid nucleates during vigorous agitation, and grows relatively slowly until a fraction solid of 0.40 to 0.60. Then, agitation is terminated, and the second stage sets in, where the remaining liquid solidifies unstirred, usually at a higher rate (quench). As a result, stircast structures are typically duplex, consisting of a coarse primary phase, embedded in a finer dendritic matrix.

The present investigation was undertaken to study the morphological changes in the microstructure of Al–6Cu, induced by stirring. In this paper, a description is given of the equipment, the experiments and the microstructures. Effects of stirring speed and cooling rate on the microstructure are investigated. To this purpose, the cell-spacings have been measured in the coarse primary phase of stircast structures and compared with secondary dendrite arm spacings in unstirred dendritic structures. The results are explained by assuming that solid growth in stirred solidification in a bulk metal liquid is cellular. In this paper, only a brief discussion of the arguments is given. In a following paper [6], a detailed interpretation of the results is given, together with results obtained in similar experiments performed with an organic analogue [7, 8].

## 2. Experimental details

### 2.1. Melting procedure

Batch-stircasting experiments were performed in an annular space between an inner rotating cylinder and an outer cylindrical material-holder, as shown in Fig. 1. The radius of the stirrer was 13 mm, and the annular gap was 3 mm. The material-holder was centred inside a cooling jacket with small holes, located opposite of the charge. The cooling jacket in turn, was mounted in an infrared heating chamber. Temperatures were measured using chromel-alumel thermocouples, at two locations, as indicated in Fig. 1. The temperatures were measured in the semi-solid metal slurry via small holes in the material-holder. The Al–6Cu alloy was heated in the

*Al–6Cu refers to the alloy Al–6 wt % Cu, which may also be written as AlCu6.

0022–2461/85 $03.00 + .12 

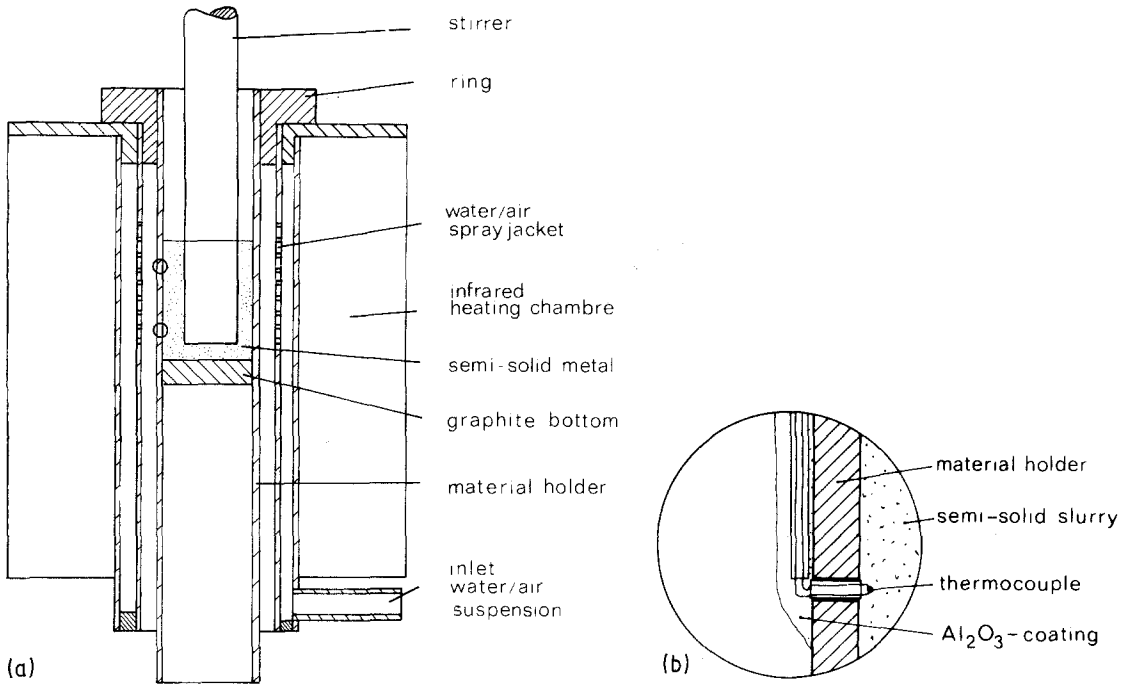


*Figure 1* (a) Schematic representation of batch-stircast apparatus. The two encircled sections are shown in detail in (b). (b) Detail of temperature measurement.

material-holder, to 993 K, i.e. to about 80 K superheat (the liquidus temperature of this alloy composition is 917 K [9]). After having reached the desired temperature, stirring and cooling started. Cooling was achieved by use of airflow. Flow velocities were not known, but different cooling rates were obtained using different initial over-pressures of air. The maximum cooling rate was achieved with a water/air-suspension, using an overpressure of 7 bars. This cooling rate was also used for quench purposes. In the solid–liquid region, the cooling rate is not constant. Therefore, it is convenient and more appropriate to use "solidification time" as a parameter to relate the results to. This is in accordance with earlier work [10]. In the liquidus region, the cooling curves appeared linear, so that cooling rates in this region can be used as a reference. In subsequent sections, the cooling rate is considered high, if $(\partial T/\partial t)_{liq} > 10\,K\,sec^{-1}$, intermediate, if $(\partial T/\partial t)_{liq} \sim 1\,K\,sec^{-1}$, and low, if $(\partial T/\partial t)_{liq} \sim 0.1\,K\,sec^{-1}$.

## 2.2. Stirring experiments with continuous cooling

A programme of stirring experiments was carried out, applying different cooling rates and stirring speeds in the solid–liquid region. To investigate the effect of the rotational speed of the stirrer upon the microstructure, experiments were performed at 250, 750 and 1500 r.p.m. In the experiments performed with the maximum cooling rate, stirring was stopped as soon as the temperature measured by the upper thermocouple fell below 893 K. The solidification time was taken as the time spent between the recorded nucleation event and the eutectic temperature. In the experiments in which cooling was initiated with air only, quench by water/air-suspension was planned at a predetermined temperature. As quench set in, the stirrer was stopped immediately, and the remaining liquid solidified unstirred.

## 2.3. Stirring experiments with interrupted cooling

In three experiments, an attempt was made to perform "isothermal" stirring for a given period of time. The cooling rate was set at maximum in the liquidus region. Having arrived at a temperature in the solid–liquid region, the cooling was stopped. The semi-solid slurry was then stirred "isothermally" for a given time after which cooling at maximum rate (quench) was continued. The stirring time, or equivalently, the solidification time, was measured between the

TABLE I Temperature drops in S–L-region, for "isothermal" stirring experiments

| Stirring time (sec) | $\Delta T$ (K) |
|---|---|
| 66 | 9 |
| 400 | 12 |
| 680 | 22 |

recorded nucleation event and the moment of quench. It must be noted that strictly isothermal stirring was difficult to achieve. After nucleation (at a certain undercooling), the temperature first increased to a maximum just below the liquidus temperature, and then decreased slowly. The temperature drop between this maximum and the moment of quench is given in Table I.

### 2.4. Reference experiments

Two reference experiments were performed, in which the samples were not stirred; one with the maximum attainable cooling rate, and another with natural cooling, i.e. without the use of air or water as a coolant.

### 2.5. Metallography

In the reference samples, secondary dendrite arm spacings were measured as schematically demonstrated in Fig. 2a. A given distance, perpendicular to the growth-direction of the secondary dendrite arms on a single primary stem, is divided by the number of arms across this distance. This procedure has also been used in earlier literature [11]. In the stirred specimens, the cell-spacings were measured as shown in Fig. 2b. The cell-spacing is taken equal to the cell-tip diameter.

## 3. Results

### 3.1. Observed microstructures

At low cooling rates, i.e. when $(\partial T/\partial t)_{liq} \sim 0.1\ K\ sec^{-1}$, the stircast structure of Al–6Cu is as shown in Fig. 3; the primary particles consist of agglomerated cells. This is in agreement with results obtained earlier by Flemings [2–4] and Joly and Mehrabian [5]. The microstructures of specimens obtained with "isothermal" stirring are similar to those obtained with slow continuous cooling. It is observed also that the amount of liquid entrapped within the primary particles decreases with increasing solidification time (Fig. 3c and d). This also is in agreement with earlier observations [5].

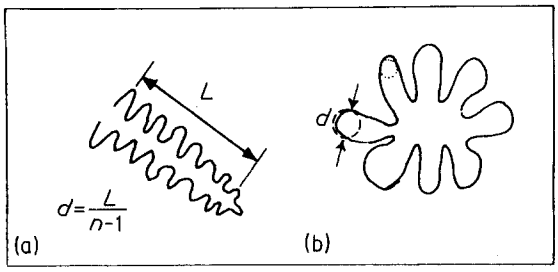


*Figure 2* Illustration of the measurement of the secondary dendrite arm spacing (*DAS*) in a dendritic structure (a), and in a stircast structure (b). $n$ is the number of secondary dendrite arms.

At intermediate cooling rates, $(\partial T/\partial t)_{liq} \sim 1\ K\ sec^{-1}$, the stircast structures are as shown in Fig. 4. These structures are usually similar to those obtained at low cooling rates, however, an important difference is the occurrence of so called rosette-type particles, see Fig. 4a. Such particles were observed before independently by Vogel *et al.* [12], Taha and El-Mahallawy [13], and Apaydin *et al.* [14]. They were not found in slowly cooled samples, probably because they are unlikely to survive the high shear rates at longer stirring times. It is suggested here, that the rosettes represent actually a form of cellular growth. Their solidification front shows a striking similarity with the cellular growth form [15]. This is equally true for the particles observed in Fig. 4b. This micrograph does not show rosettes, but particles which consist of radially grown cells. Obviously, the rosettes are fragmented in time, to form other particles with a cellular growth front.

At high cooling rates, $(\partial T/\partial t)_{liq} > 10\ K\ sec^{-1}$, the observed stircast structures are as shown in Fig. 5. Fig. 5a shows the structure at low magnification; Fig. 5b shows another sample obtained under the same experimental conditions, at higher magnification. Often in these structures, rosette-type particles can be observed, reduced in size when compared to the rosettes observed at intermediate cooling rates. The rosettes may appear damaged or fragmented by the mechanical action of the stirrer. Concluding, the following observations have been made:

1. The stircast structure of Al–6Cu is non-dendritic at all applied cooling rates; it is finer at high cooling rates.

2. At high and intermediate cooling rates, both rosette-type particles and particles

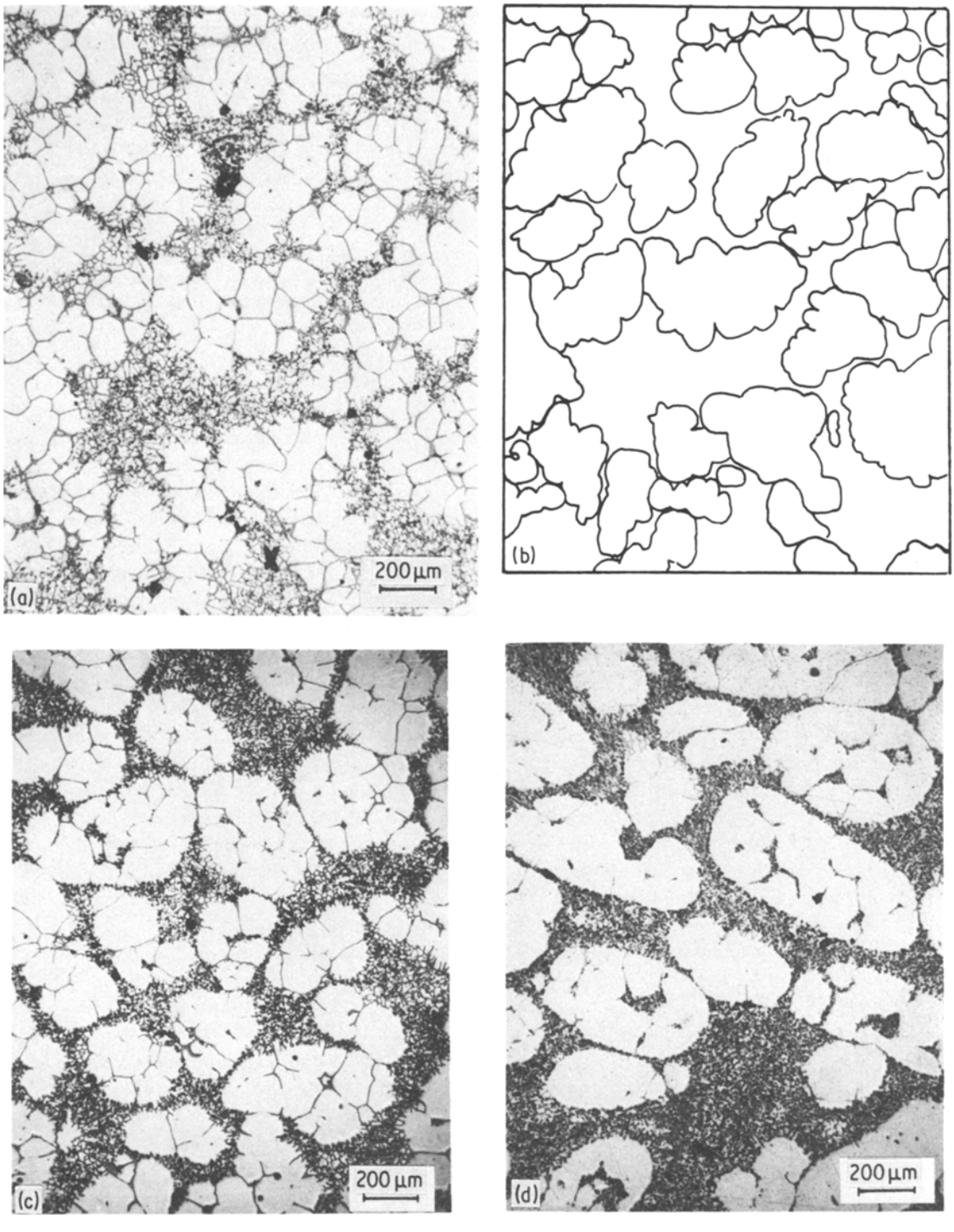


*Figure 3* Stircast structures of Al–6Cu, obtained at low cooling rates, $(\partial T/\partial t)_{liq} \sim 0.1\,K\,sec^{-1}$). The rotational speed of the stirrer, and the solidification time in the solid–liquid region in each case were respectively: (a) 250 r.p.m., 780 sec, (b) illustration of particle countings in (a), (c) 750 r.p.m., 540 sec, (d) 750 r.p.m., 2700 sec.

consisting of radially grown cells are observed. These show a striking resemblance with the cellular growth type.

3. At low cooling rates, i.e. with longer stirring times, the particles observed consist of agglomerated cells.

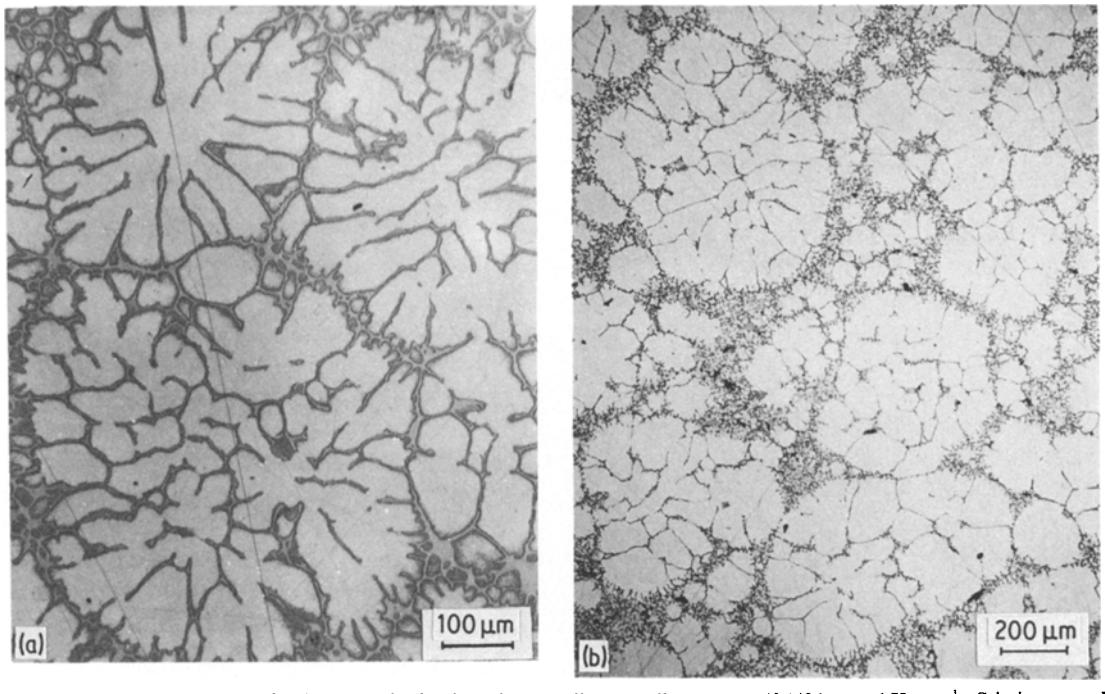


*Figure 4* Stircast structures of Al–6Cu, obtained at intermediate cooling rates, $(\partial T/\partial t)_{liq} \sim 1\,K\,sec^{-1}$. Stirring speed 1500 r.p.m. (a) Typical rosette-type particles. Solidification time in S–L is 54 sec. (b) Primary particles with cellular growth front. Solidification time in S–L-region is 400 sec.

4. The amount of liquid entrapped between the cells decreases with increasing solidification time.

### 3.2. Effect of the rotational speed of the stirrer

The effect on structure of the rotational speed of the stirrer was investigated by primary particle counting, and by measuring primary particle size. Particle countings and particle size measurements were made only in samples obtained with low and intermediate cooling rates, because there is no unambiguous manner to distinguish individual particles in samples obtained with high cooling rate. An example is shown in Fig. 3b. It is sometimes difficult to determine which cells belong to a particle. The particles are then determined as approximate ellipses, with a minor and a major axis. This procedure was employed for specimens stirred at 250, 750 and 1500 r.p.m., of which examples are shown in Fig. 3. By measuring minor and major axes, the particle size distributions shown in Fig. 6 were obtained. The relative frequency of the lengths of the minor axes is plotted in the positive direction, and that of the lengths of the major axes in the negative direction. The results are shown for 250 and 1500 r.p.m., for short and long stirring times. A similar result, not shown here, was obtained from samples stirred at 750 r.p.m. The figure shows that the relative frequency of small particles is not significantly greater at high stirring speeds. Nor is the relative frequency of large particles significantly greater at low stirring speeds. Therefore it is concluded, that the stirring speed (shear rate) does not have a significant effect upon primary particle size.

Apart from the particle size distribution, the stircast structure is described by the number of particles per unit volume. Here, the number of particles per square mm, $M$ was determined. The results of these countings are listed in Table II. In this table, also $f_{sq}$, the volume fraction solid at the quench temperature was determined, using the Scheil equation. To see if the calculated solid fraction is meaningful with respect to the observed fraction primary particles, the total area taken by the particles was measured, excluding the dendritic zone on top of the particle surfaces, because it was assumed that this zone is formed during quenching. The entrapped (intercellular) liquid was included only when it constituted a thin film. Thus, the so called effective fraction solid was determined,

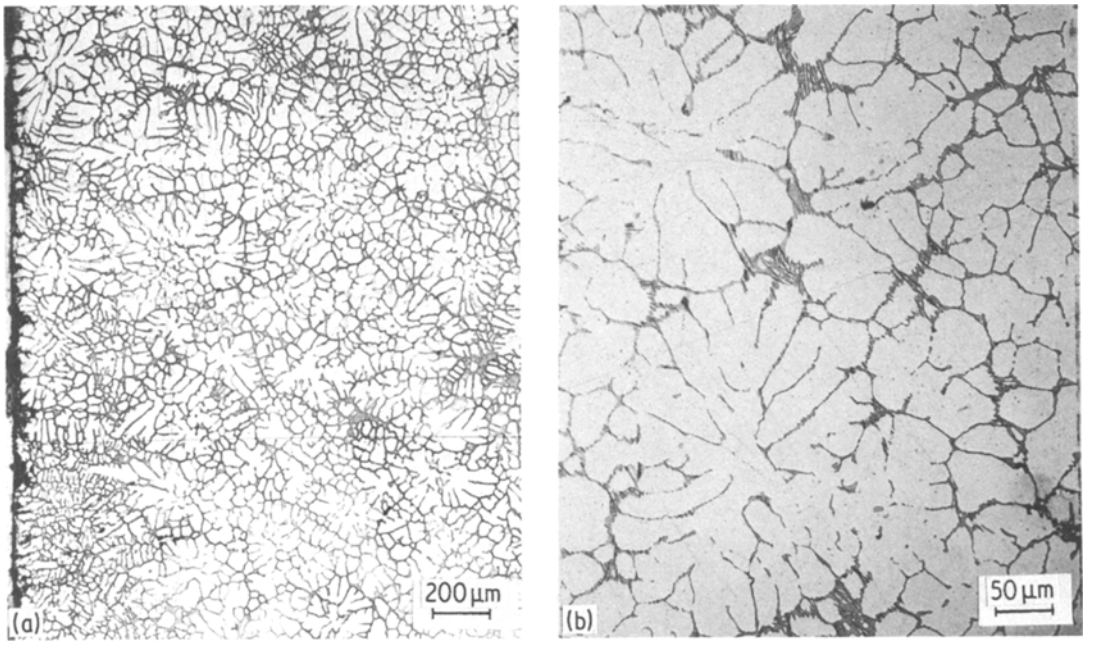


*Figure 5* Stircast structures of Al–6Cu, obtained at high cooling rate, $(\partial T/\partial t)_{liq} > 10\,K\,sec^{-1}$. Stirring speed 1500 r.p.m., solidification time in S–L-region 8 sec. (a) Structure at low magnification. (b) Rosette-type particles at higher magnification.

which is given in Table II as $f_{se}$. It is found that the effective fraction solid can vary between $f_{sq}$ and $1.66f_{sq}$. This gives an indication of the amount of entrapped liquid. In Fig. 7, $M$, the number of particles per square mm, is shown as a function of the effective fraction solid $f_{se}$, for different stirring speeds. This figure shows that $M$ is not changed at different stirring speeds. So, it is concluded, that the stirring speed does not have a strong influence on the number of particles per unit volume.

### 3.3. Cell-spacing in stirring experiments

The cells of which the spacings have been measured as shown schematically in Fig. 2b, are considered as the structural units from which the primary particles in a stircast structure have apparently agglomerated. Only the spacings of the cells which are in contact with the remaining "liquid" which surrounds the primary particles, were measured. The measurements were made in different cross-sections of a cast sample: (1) parallel, and near to the surface of the stirrer, (2) parallel, and near to the (chilled) surface of the material holder, (3) transverse cross-sections. Over a range of observations, the spacings in the different cross-sections were found equal within the standard deviation. The average values of the cell-spacings are given in the last column of Table III. The second and third column give the

TABLE II Number of particles per square mm, ($M$), and effective fraction solid, $f_{se}$, measured under the various experimental conditions ($f_{sq}$ is fraction solid at quench temperature, calculated using the Scheil equation).

| Specimen number | Stirring speed (r.p.m.) | Solidification time (sec) | Quench temperature (K) | $f_{sq}$ | $f_{se}$ | $M$ ($mm^{-2}$) |
|---|---|---|---|---|---|---|
| 1 | 250 | 228 | 908 | 0.38 | 0.63 | 3.6 |
| 2 | 250 | 420 | 901 | 0.53 | 0.66 | 5.3 |
| 3 | 250 | 780 | 908 | 0.38 | 0.63 | 7.6 |
| 4 | 250 | 1860 | 893 | 0.63 | 0.73 | 7.5 |
| 5 | 750 | 540 | 896 | 0.60 | 0.67 | 5.3 |
| 6 | 750 | 2700 | 896 | 0.60 | 0.62 | 6.1 |
| 7 | 1500 | 360 | 903 | 0.49 | 0.57 | 3.7 |
| 8 | 1500 | 2010 | 903 | 0.49 | – | 5.6 |

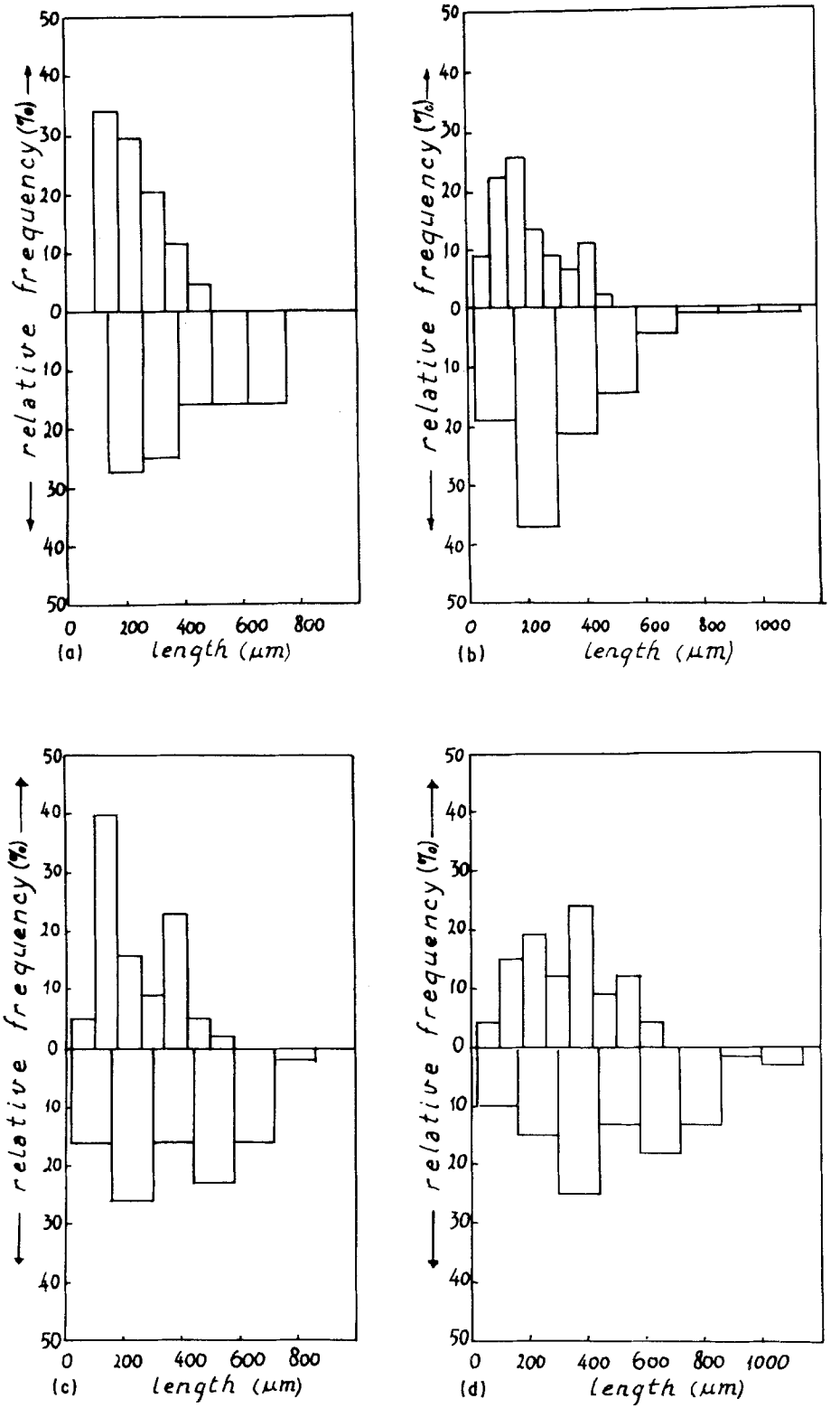


*Figure 6* Relative frequency distributions of primary particle size in stircast Al–6Cu. The lengths of the minor axes are plotted in the positive direction; those of the major axes in the negative direction. Stirring speed 250 r.p.m. (a) $t_s$ = 780 sec, (b) $t_s$ = 1860 sec; 1500 r.p.m. (c) $t_s$ = 2010 sec, (d) 360 sec.

TABLE III Results of cell-spacing measurements

| Specimen number | Stirring speed (r.p.m.) | Solidification time (sec) | Average cell-spacing ($\mu$m) |
|---|---|---|---|
| 1 | 1500 | 8.4 | 25 |
| 2 | 1500 | 8.8 | 28 |
| 3 | 1500 | 9.0 | 34 |
| 4 | 1500 | – | 27 |
| 5 | 1500 | – | 27 |
| 6 | 1500 | 15 | 29 |
| 7 | 1500 | 26 | 39 |
| 8 | 1500 | 36 | 38 |
| 9 | 1500 | 54 | 54 |
| 10* | 1500 | 66 | 67 |
| 11 | 250 | 228 | 109 |
| 12 | 1500 | 252 | 103 |
| 13 | 1500 | 360 | 139 |
| 14* | 1500 | 400 | 153 |
| 15 | 250 | 420 | 123 |
| 16* | 1500 | 680 | 206 |
| 17 | –† | 7.0 | 27 |
| 18 | –† | 380 | 68 |

*"isothermal" stirring experiment.
† Reference experiment (no stirring).

stirring speed and the solidification time respectively. In Fig. 8, the average cell-spacings are plotted as a function of the total solidification time. It is assumed that the points are on a straight line in a double logarithmic graph, in correlation with work by Bower *et al.* [16] and Kattamis *et al.* [17, 18]. Using the least squares method, the following relation was found:

$$\log \langle d \rangle = 0.42 \log t_s + 1.01 \qquad (1)$$

where $\langle d \rangle$ is the cell-spacing ($\mu$m), and $t_s$ is the solidification time (sec). The slope of this line is approximately equal to that of Bower's line (0.39 [16]), which is also shown in Fig. 8, for comparison (solid line). Relation 1 is valid for all stirring speeds applied, which implies that the cell-spacing is independent of the stirring speed. Fig. 8 shows that the cell-spacing of the primary solidified phase in the stirred samples is greater than the secondary dendrite arm spacing in non-stirred samples, at equal solidification times.

Note finally, that the total solidification time, for the stirred samples is equivalent with the local solidification time as defined with Bower's result. This requires some further explanation. In Bower's work [16], the local solidification time is defined as the time required by the growth front to pass a distance equal to the length of the mushy zone. In stircasting, the mushy zone is extended to the total volume of the stirred semi-solid slurry. Therefore, the total solidification time (which is approximately equal to the stirring time) is equivalent with the local solidification time for a primary particle.

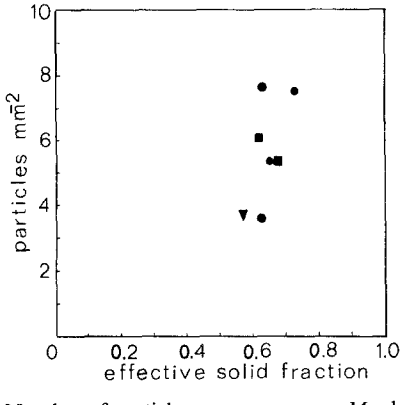


*Figure 7* Number of particles per square mm, $M$, plotted as a function of the effective fraction solid, $f_{se}$. Stirring speeds of ●250, ■ 750 and ▼ 1500 r.p.m.

### 3.4. Secondary dendrite arm spacing in reference experiments

The structures of the reference samples (not stirred) are shown in Fig. 9. In these structures, the secondary dendrite arm spacing ($DAS$) was measured, as described in Section 2.5. In Fig. 8, the secondary $DAS$ measured as a function of the total solidification time, is compared to the cell-spacings measured in the stirred samples. It is seen that the points of the reference experiments lie somewhat below Bower's line. This result is expected, because in the non-stirred samples the local solidification time is actually smaller than the measured total solidification time.

## 4. Discusssion

Vogel and Cantor [19] have shown theoretically, that stirring destabilizes the solid–liquid interface of a primary crystal growing in a bulk liquid, and thus favours the dendritic type of growth. Therefore, secondary dendrite-arms which are detached in early stages of solidification, are expected to continue to grow dendritically. However, stircast structures observed up to date are typically non-dendritic. As an explanation, Doherty *et al.* [12, 20] have suggested a dendrite fragmentation mechanism, in combination with a stabilizing influence, which arises from the interaction of thermal

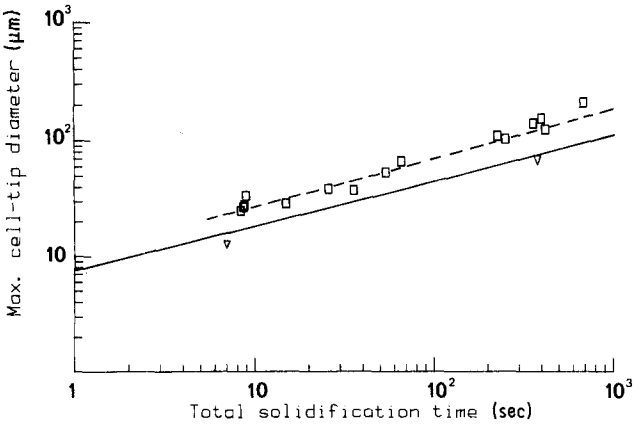


*Figure 8* Cell spacing in stircast structures plotted as a function of the total solidification time. Squares indicate average cell-spacings obtained in stirring experiments, for which the dashed line was obtained as the best fit using the least squares method. Triangles represent results of reference experiments (non-stirred samples). Bower's result (solid line) is shown for comparison.

diffusion fields of fragmented particles. These authors [19, 20] clearly assume, that stirred solidification of metal alloys is dendritic in the initial stage. However, the results presented here indicate, that the growth of primary particles is not dendritic, but cellular, already in an early stage of the solidification. Experimental evidence in support of this, are the rosette-type particles, see Fig. 5b, and particles which consist of radially grown cells, such as in Fig. 4b. These particles have apparently grown "spherically" cellular. The increased cell-spacings observed in stircast structures, are in agreement with this assumption when interpreted as a consequence of a more stable morphological type of growth. The cellular growth type of solid in the bulk of stirred metal liquids can be made further plausible on the basis of qualitative arguments. The Prandtl-number of liquid metals is small ($\sim 0.01$), indicating that the thermal boundary layer of a primary particle is much greater than its hydrodynamic boundary layer. As a result of convection, temperature differences across the hydrodynamic boundary layer will be small. The ratio of the thermal gradient at the solid–liquid interface in the liquid, $G$, and the growth rate, $R$, is small at the onset of the solidification in the bulk, and approaches zero, due to the interaction of thermal diffusion fields of the individual particles, as these grow and become more numerous. This condition leads to the suggestion, that solid growth will be cellular. In a following paper [6], these arguments are discussed in greater detail.

## 5. Conclusions

1. The stircast structure is non-dendritic at all applied cooling rates; it is finer at high cooling rates.

2. The rotational speed of the stirrer does not

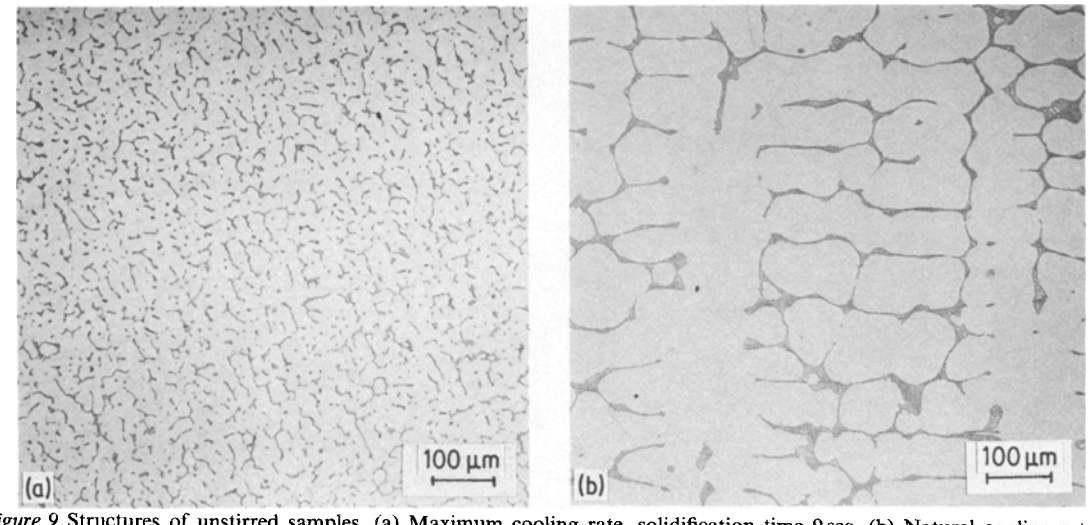


*Figure 9* Structures of unstirred samples. (a) Maximum cooling rate, solidification time 9 sec. (b) Natural cooling rate, solidification time 380 sec.

influence the cell-spacing, and does not have a significant effect on the particle size distribution, nor on the number of particles per unit volume.

3. The stircast structure shows typical characteristics of the cellular morphological type of growth in the rosette-type particles, and in particles consisting of radially grown cells. The observed increase in the cell-spacings is in agreement with cellular growth, as this is a more stable morphological type of growth.

## Acknowledgement

The authors are grateful to W. H. Kool and A. J. Dalhuijzen for their critical reading of the manuscript, and to BIRA, Stichting Bevordering Industriele Research Aluminium-industrie (Industrial Aluminium Research Foundation), The Netherlands, for financial support.

## References

1. J. M. M. MOLENAAR, F. W. H. C. SALEMANS and L. KATGERMAN, *J. Mater. Sci.* **20** (1985) 700.
2. M. C. FLEMINGS, R. G. RIEK and K. P. YOUNG, *Mater. Sci. Eng.* **25** (1976) 103.
3. *Idem, AFS Int. Cast Met. J.* **1** (1976) 11.
4. M. C. FLEMINGS *et al.* "Rheocasting", Proceedings of a Workshop, Metals and Ceramics Information Center, Batelle's Columbus Laboratories, Columbus Ohio, 1978, edited by R. D. French and F. S. Hodi (Metals and Ceramics Information Center, Columbus).
5. P. A. JOLY and R. MEHRABIAN, *J. Mater. Sci.* **11** (1976) 1393.
6. J. M. M. MOLENAAR, R. J. SMEULDERS and L. KATGERMAN, *J. Mater. Sci.* **21** (1986) in press.
7. R. J. SMEULDERS, F. H. MISCHGOFSKY and H. J. FRANKENA, Proceedings of the International Conference on Optical Techniques in Process Control, The Hague, The Netherlands, June 1983, edited by H. S. Stephens and C. A. Stapleton (British Hydromechanics Research Association, Cranfield, 1983) p. 265.
8. R. J. SMEULDERS, PhD thesis, Delft University of Technology, Department of Applied Physics, Delft, The Netherlands, 22 November, 1984.
9. M. H. BURDEN and J. D. HUNT, *J. Cryst. Growth* **22** (1974) 99.
10. M. C. FLEMINGS, "Solidification Processing" (McGraw-Hill, New York, 1974) p. 148.
11. J. A. HOWARTH and L. F. MONDOLFO, *Acta Metall.* **10** (1962) 1037.
12. A. VOGEL, R. D. DOHERTY and B. CANTOR, Proceedings of the International Conference on Solidification and Casting of Metals, University of Sheffield, July 1977 (The Metals Society, London, 1979) p. 518.
13. M. A. TAHA and N. A. EL-MAHALLAWY, Proceedings of the 46th International Foundary Congress, Madrid, 1979 (Asociacion Tecnica de Investigacion de Fundicion, Madrid, 1979) paper 15.
14. N. APAYDIN, K. V. PRABHAKAR and R. D. DOHERTY, *Mater. Sci. Eng.* **46** (1980) 145.
15. R. M. SHARP and A. HELLAWELL, *J. Cryst. Growth* **11** (1971) 77.
16. T. F. BOWER, H. D. BRODY and M. C. FLEMINGS, *Trans. AIME* **236** (1966) 624.
17. T. Z. KATTAMIS, J. C. GCOUGHLIN and M. C. FLEMINGS, *ibid.* **239** (1967) 1504.
18. K. H. CHIEN and T. Z. KATTAMIS, *Z. Metallkde* **61** (1970) 475.
19. A. VOGEL and B. CANTOR, *J. Cryst. Growth* **37** (1977) 309.
20. R. D. DOHERTY, H. I. LEE and E. A. FEEST, *Mater. Sci. Eng.* **65** (1984) 181.

*Received 3 May 1984*
*and accepted 20 May 1985*